Inorganic Chemistry

pubs.acs.org/IC

Article

Thermodynamic Stability, Structure, and Optical Properties of Perovskite-Related $CsPb_2Br_5$ Single Crystals under Pressure

Viktoriia Drushliak and Marek Szafrański*

Cite This: *Inorg. Chem.* 2022, 61, 14389−14396

Read Online

ACCESS | Metrics & More | Article Recommendations | Supporting Information

ABSTRACT: $CsPb_2Br_5$ belongs to all inorganic perovskite-related quasi-two-dimensional materials that have attracted considerable attention due to their potential for optoelectronic applications. In this study, we solve numerous controversies on the physical properties of this material. We show that optical absorption in the visible spectrum and green photoluminescence are due to microcrystallites of the three-dimensional $CsPbBr_3$ perovskite settled on the $CsPb_2Br_5$ plates and that carefully cleaned crystal plates are devoid of these features. The high-pressure structural and spectroscopic experiments, performed on the single crystals free of $CsPbBr_3$ impurities, evidenced that the layered tetragonal structure of $CsPb_2Br_5$ is stable at least up to 6 GPa. The absorption edge is located in the ultraviolet at around 350 nm and continuously red shifts under pressure. Moderate band gap narrowing is well correlated to the pressure-induced changes in the crystal structure. Although the compressibility of $CsPb_2Br_5$ is much higher than for $CsPbBr_3$, the response in optical properties is weaker because the Pb−Br layers responsible for the optical absorption are much less affected by hydrostatic pressure than those built of Cs^+ cations. Our study clarifies the confusing data in the literature on the optical properties and thermodynamic stability of $CsPb_2Br_5$.

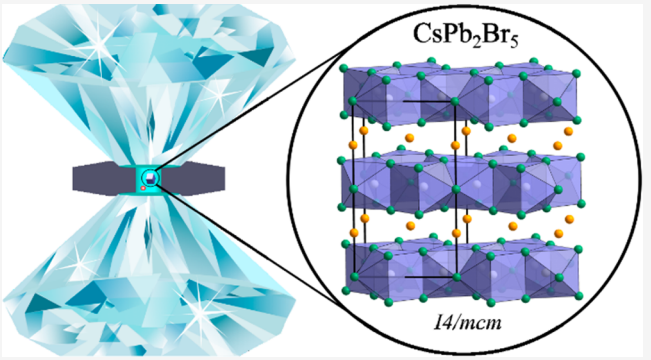

1. INTRODUCTION

In the recent decade, organic−inorganic perovskite semiconductors have attracted unprecedented attention from the scientific community.[1] This interest stems from their excellent photovoltaic and optoelectronic properties combined with easy and low-cost fabrication. However, the long-term stability problems in the operating environment have not yet been solved. In this area, a very promising research direction is connected with all-inorganic perovskites that exhibit better resistance to atmospheric conditions, while their optoelectronic parameters are comparable to those of their hybrid counterparts, as was demonstrated for $CsPbBr_3$.[2] Cesium lead bromide can crystallize in orange (three-dimensional, 3D) and white (one-dimensional, 1D) forms, but also with different stoichiometries,[3] forming low-dimensional structures: Cs_4PbBr_6, often termed a zero-dimensional perovskite (0D), and $CsPb_2Br_5$, exhibiting a two-dimensional architecture (2D). These low-dimensional perovskite-related materials have gained remarkable interest because of strong photoluminescence (PL) in the visible spectrum,[4,5] reported recently, which opens prospects for applications in light-emitting diodes,[6] lasers,[7] and photodetectors.[8,9]

Here, we present a systematic structural and optical spectroscopic high-pressure study performed on pure single crystals of $CsPb_2Br_5$. In the tetragonal structure of $CsPb_2Br_5$, the bicapped trigonal prisms $PbBr_8$ are connected by faces into layers perpendicular to the *c*-axis. These Pb−Br layers are sandwiched between layers composed of Cs^+ cations.[10,11] The crystal structure is shown in Figure 1. The quasi-2D character of the structure should result in a wider band gap compared to that of the 3D orange form of $CsPbBr_3$ for which the energy gap E_g = 2.34 eV[12] (λ = 530 nm). Indeed, in the original work,[3] published by Wells in 1893, $CsPb_2Br_5$ is characterized as a white powder, indicating an absorption edge in the ultraviolet region. Therefore, the location of the absorption edge in the visible spectrum around 515−525 nm in numerous papers[5,6,8,13] is highly questionable because in that case the crystal could not be colorless. Furthermore, theoretical calculations of the electronic structure indicate that the energy gap in $CsPb_2Br_5$ is of indirect type,[5,10,14] and for that reason, strong PL should be excluded. In fact, detailed studies of carefully prepared material showed that pure $CsPb_2Br_5$ does not absorb light in the visible region and is PL inactive.[10,14,15] The controversial strong green emission was discussed by

Received: June 28, 2022
Published: September 1, 2022

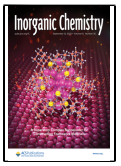

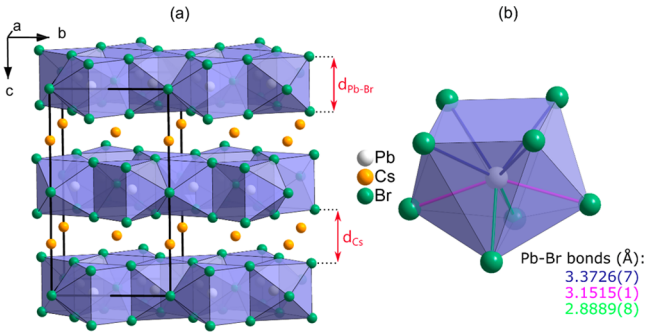

Figure 1. (a) Crystal structure of $CsPb_2Br_5$ with the thickness of the Pb−Br and Cs layers marked by the arrows and (b) the bicapped trigonal prism $PbBr_8$ being the building unit of the Pb−Br layers. The three different Pb−Br distances and their values determined under ambient conditions are marked with different colors.

several groups, which indicated possible origins of this emission, such as impurities of the orange phase of $CsPbBr_3$ mixed with $CsPb_2Br_5$,[16] $CsPbBr_3$ nanocrystals embedded in $CsPb_2Br_5$ microplates,[17] amorphous lead bromide ammonium complexes present on the surface of the nanosheets,[18] or intrinsic crystal defects.[19] It appears that the methodology of $CsPb_2Br_5$ preparation is crucial in this respect because even a small amount of $CsPbBr_3$ admixture strongly affects the optical properties of the material obtained. This is clearly seen in previously published studies,[5,6,8,13] where on the basis of the standard powder X-ray diffraction analysis the material is defined as "pure", while its absorption edge and PL properties are evidently dominated by the presence of the orange form of $CsPbBr_3$, and they are dramatically different from those of the truly pure substance.[10,15] Although from the point of view of optoelectronic applications the strongly light-emitting two-phase material is very attractive, the physical properties determined for such material and their assignment to the pure form lead to misleading information and errors of interpretation of the data.

In this study, we report the response of the $CsPb_2Br_5$ structure to hydrostatic pressure and the related changes in the optical properties of the crystal. Special emphasis was placed on the synthesis and crystallization procedures. We show that our results obtained for pure single crystals are completely different from those published previously.[13]

2. MATERIALS AND METHODS

2.1. Chemicals. Cesium carbonate (Aldrich, 99%), hydrobromic acid for analysis (Acros Organics, 48% solution in water), and lead(II) acetate trihydrate (Aldrich, 99.999%) were purchased and used without further purification. The water was purified by double distillation.

2.2. Synthesis of $CsPb_2Br_5$. Cesium bromide and lead(II) bromide were obtained by reactions of hydrobromic acid with cesium carbonate and lead(II) acetate trihydrate. The stoichiometric amounts of CsBr and $PbBr_2$ were dissolved in hot water acidified with HBr. Slow cooling of the solution to room temperature resulted in the crystallization of thin $CsPb_2Br_5$ plates. The precipitated crystals were filtrated, washed with hexane, and dried. We also performed a series of crystallizations to determine the optimal conditions for growing the good-quality pure crystals. In these experiments, the amount of HBr acid in the solution and/or the CsBr:$PbBr_2$ ratio were modified.

2.3. Calorimetric and Thermogravimetric Analysis. The thermal stability of $CsPb_2Br_5$ was studied by the thermogravimetric analysis method (TGA) using a TGA Q50 instrument (TA Instruments) and by differential scanning calorimetry (DSC) with a

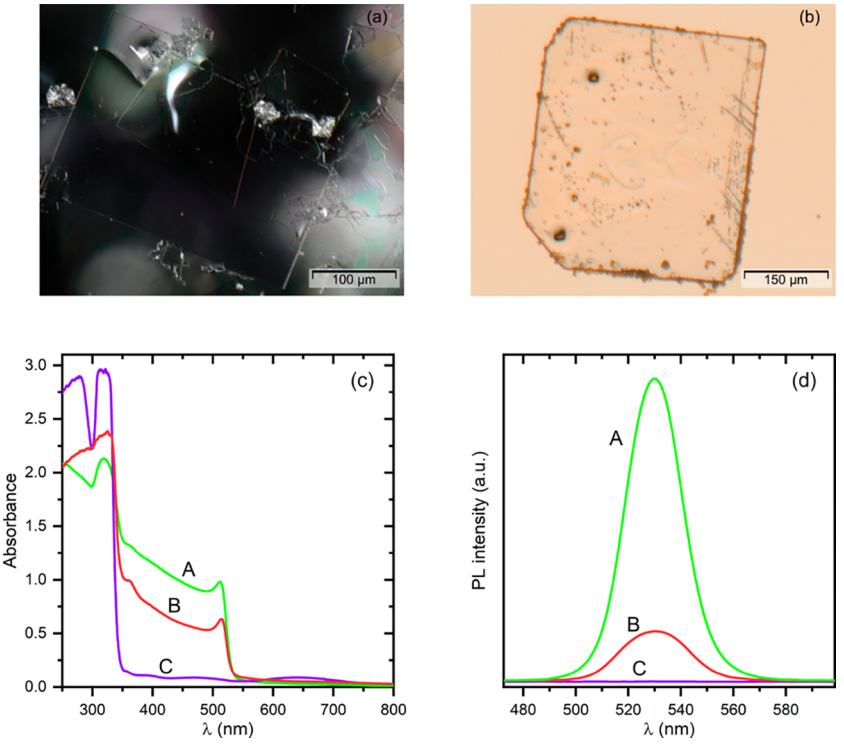

Figure 2. Photographs of crystals taken from the solution: (a) after washing and drying (reflected light) and (b) after drying only, with visible microcrystals of orange $CsPbBr_3$ crystallized on the surface plate (transmitted light). Absorption (c) and photoluminescence (d) spectra of $CsPb_2Br_5$. The spectra recorded for two different as-grown (unwashed) crystal plates are marked by A and B, and the spectra of the cleaned plate are marked by C.

https://doi.org/10.1021/acs.inorgchem.2c02253
Inorg. Chem. 2022, 61, 14389−14396

Q2000 calorimeter (TA Instruments). DSC experiments were performed on as-grown crystals while TGA runs were measured on powdered samples, both at a temperature change rate of 10 K min^{-1}.

2.4. Single-Crystal High-Pressure X-ray Diffraction. A Merrill-Bassett diamond anvil cell (DAC)[20] equipped with diamond anvils (type Ia, 800 μm culets) supported on steel discs with conical windows was used for single-crystal X-ray diffraction (SCXRD) high-pressure experiments. The single crystal of $CsPb_2Br_5$ and the ruby chip for pressure calibration were glued to the culet of one anvil and placed into the spark-eroded hole in the tungsten gasket (initial thickness 250 μm, hole diameter 350−380 μm). The chamber was filled with isopropanol as a pressure medium, ensuring hydrostatic conditions up to ∼4.2 GPa.[21] The pressure inside the DAC was monitored by using the ruby fluorescence method,[22] before and after each measurement. The overall pressure uncertainty was <0.03 GPa. All SCXRD measurements were performed at room temperature by using an Oxford Diffraction Gemini A Ultra diffractometer operating with graphite-monochromated Mo Kα radiation (λ = 0.71073 Å). Data were collected and processed by using CrysAlisPro software.[23] The structures were solved and refined by using SHELX programs.[24] Crystallographic information files (CIFs) for $CsPb_2Br_5$ structures determined under different pressures (2176587−2176600) have been deposited in the Inorganic Crystal Structure Database.

2.5. Optical Measurements. For high-pressure optical spectroscopic measurements, diamond anvils type IIa, supported by tungsten carbide seats with conical windows, were used. The hydrostatic liquid and other experimental details were the same as in the case of diffraction experiments. The pressure dependence of the absorption edge was measured on a 3.9 μm thick plate and on a nanosheet of the average thickness 30 nm, which was grown in situ on the diamond culet surface. The thickness of the nanosheet was determined with the atomic force microscopy (AFM) technique, whereas an interference method combined with optical microscopy was used to measure the thickness of the microplates (see Figure S1). Absorption and diffuse reflectance spectra were recorded by a Jasco MSV-5100 microscopic spectrophotometer. The absorption spectra were collected from the small area of the crystals of 30 μm in diameter by using a continuous speed of 200 nm min^{-1} and a spectral bandwidth of 5 nm.

PL spectra were measured with a homemade attachment to the Jasco MSV-5100 spectrophotometer, where a xenon lamp served as an excitation source in the spectral range 320−500 nm, and a Spectra Academy SV2100 spectrometer was applied for analysis of the spectrum emitted by the sample. All spectroscopic measurements were performed at room temperature.

3. RESULTS AND DISCUSSION

3.1. Characterization of the Material. An overview of the papers published on $CsPb_2Br_5$ shows a large diversity of methods applied for the synthesis and crystallization of this material.[3,5,6,10,14,16,25−28] Many of these studies were focused on the preparation of microcrystals or nanocrystals by triggering off a sudden crystallization through a hot injection method.[8,13,14,17,18,25] In such syntheses, the control of a single-phase crystallization is limited, especially when the substrates can form structures of different stoichiometries. For the purposes of this work, we used the simplest method of crystallization from an aqueous solution, which was already described by Wells in 1893[3] and has been successfully used recently.[11,15] The obtained crystals were colorless and of good optical quality (Figure 2a). Their layered tetragonal symmetry structure was confirmed by SCXRD measurements (Figure 1; for details, see also Table S1). The space group symmetry *I*4/*mcm* and the lattice parameters $a = b = 8.4931(1)$ Å and $c = 15.1786(3)$ Å are consistent with the previously reported data.[29] According to our DSC and TGA measurements, this structure is stable at least between 95 and 625 K (see Figures S2 and S3). In particular, our study did not confirm the thermal anomaly observed previously at 341.5 K.[30] The only DSC anomaly was detected at 625 K, where the crystal melts.

The purity of the crystals grown, and especially the presence of $CsPbBr_3$ admixture, was monitored by the absorption spectroscopy method. The orange form of $CsPbBr_3$ exhibits strong absorption below ca. 530 nm, and even trace amounts of this substance in the studied material are clearly reflected in the absorption spectrum. Therefore, this method is much more sensitive than the commonly used powder X-ray diffraction. The crystallizations performed from the water solutions, acidified with different amounts of HBr, showed that all of the obtained and carefully cleaned crystals exhibit the same optical properties; that is, they are colorless and transparent, their absorption edge is located below 350 nm, and they are devoid of green PL (see plots C in Figure 2c,d). This also concerns the crystals grown from the strongly acidified solution, which crystallized together with the orange form of $CsPbBr_3$. The only visible difference was in the thickness of the plates, which clearly increased with the amount of acid in the solution. This is a result of the better solubility of the substrates and their higher concentrations in the acidified solution. It is well-known that the 3D $CsPbBr_3$ perovskite crystallizes in water solution only at a sufficiently high concentration of HBr; otherwise, $CsPb_2Br_5$ is formed,[3] regardless of the 1:1 stoichiometry of $CsBr:PbBr_2$ in the solution. Our experiments confirmed that also in solutions containing an excess of CsBr the crystals of $CsPb_2Br_5$ were obtained in pure form. Thus, it is evident that $CsPb_2Br_5$ crystallizes without any inclusions of $CsPbBr_3$, even in solutions of disturbed stoichiometry. However, it should be noticed that the crystals harvested from the solution have to be carefully washed and dried to remove the remaining solution. Living these remains on crystal plates leads to an increase in HBr concentration in the droplets of the mother liquor due to water evaporation, and finally it results in the precipitation of $CsPbBr_3$ micro- and nanocrystallites on the surface of $CsPb_2Br_5$ crystals (Figure 2b). Therefore, such "unwashed" crystal plates absorb light in the visible spectrum below 520−530 nm and exhibit strong green PL; that is, they show typical characteristics of the orange form of $CsPbBr_3$. This is illustrated in Figure 2c,d where the absorption and PL spectra of two as-grown unwashed plates (A, B) and of the cleaned plate (C) are shown. The intensity of PL is correlated to the absorbance of the samples in the spectral range 350−550 nm, which clearly depends on the amount of $CsPbBr_3$ on the crystal surfaces. All our further experiments were performed on pure $CsPb_2Br_5$ crystals.

A review of data from the literature shows that the optical spectrum of $CsPb_2Br_5$ has been the subject of numerous studies, but only very few experiments have been performed for noncontaminated samples. In Figure 3 we compare the spectrum measured by the diffuse reflectance method with that obtained from the optical absorption measurements on the 30 nm thick sheet. The reflective spectrum is presented in the form of a normalized Kubelka−Munk function,[31] $F(R_\infty) = \alpha/S = (1 - R_\infty)^2/2R_\infty$, where α is the absorption coefficient, S is the scattering coefficient of the powdered sample, and R_∞ is the diffuse reflectance of an infinitely thick layer. The two peaks visible in this spectrum at 336 nm (3.69 eV) and 307 nm (4.04 eV) are in excellent agreement with the earlier reflectance data.[11] However, a comparison with the conventional absorption spectrum reveals essential differences, as the absorption peaks are clearly blue shifted to 320 nm (3.87 eV)

https://doi.org/10.1021/acs.inorgchem.2c02253
Inorg. Chem. 2022, 61, 14389−14396

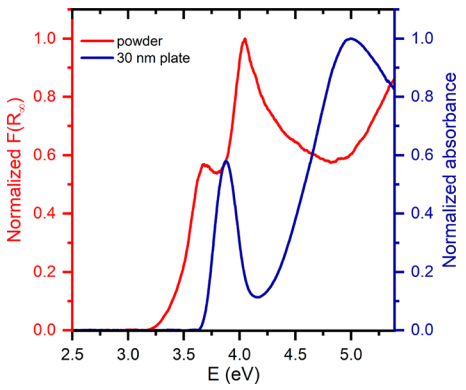

Figure 3. Normalized Kubelka–Munk function for powdered sample (left *Y*-axis) and normalized absorbance for 30 nm thick plate (right *Y*-axis) as functions of energy.

and 255 nm (4.86 eV), respectively. This discrepancy can indicate a substantial difference between the bulk electronic states, responsible for the transient absorbance, and the surface electronic states that contribute mainly to the reflection. For comparison purposes, we also measured the diffuse reflectance and absorption spectra of the 3D perovskite $MAPbBr_3$. These spectra, plotted in Figure S4, show the same trend as in the case of $CsPb_2Br_5$. Therefore, it is evident that the energy gaps determined from the absorption and reflectance data can differ considerably. It is worth noting that the onset of 3D lead-halide perovskites absorption is dominated by excitonic absorption,[32] and it is also characteristic of 2D $CsPb_2Br_5$, for which the excitonic band at 320 nm determines the absorption edge of the crystal.

3.2. Pressure Dependence of Structural Parameters of $CsPb_2Br_5$. The SCXRD data were collected in the pressure range to 4.2 GPa. As shown in Figure 4, the hydrostatic compression of the crystal results in a continuous shortening of the lattice parameters and a decrease in the unit cell volume. The monotonic contraction of the crystal, as well as the preservation of the space group symmetry *I*4/*mcm* in the whole studied pressure range, testifies that this layered structure is highly stable not only in a wide temperature range but also under pressure. The lack of structural transformation is surprising in contrast to the recently published high-pressure study of $CsPb_2Br_5$, where an isostructural phase transition was postulated at 1.6 GPa,[13] associated with a stepwise change in the lattice parameters and ∼3% decrease in the unit-cell volume. However, it should be noted that in this study the measurements by powder XRD were performed by using silicon oil as a pressure medium, which is hydrostatic to ∼1 GPa only. In this case, the pressure dependence of the lattice parameters can be strongly distorted by the nonhydrostatic conditions of the experiments. For the sake of comparison, our $V(p)$ data are plotted in Figure S5a together with those previously reported in ref 13. The most striking is a deepening discrepancy between these two data sets as the pressure increases. For example, at atmospheric pressure the unit-cell volume determined from our single-crystal data (V = 1092 Å^3) is very close to that measured by the powder diffraction method in ref 13 (V = 1088 Å^3), while under a pressure of 4 GPa the corresponding values strongly diverge (925 vs 965 Å^3, respectively). Moreover, it is worth noting that the discontinuities in the lattice parameters derived from the powder diffraction data are in fact hardly correlated to the smooth changes in the presented diffraction patterns,[13] and therefore the reported phase transition seems to be highly questionable.

The experimental $V(p)$ data plotted in Figure 4b were fitted by the third-order Birch–Murnaghan equation of state:[33]

$$p(V) = \frac{3B_0}{2}\left[\left(\frac{V_0}{V}\right)^{7/3} - \left(\frac{V_0}{V}\right)^{5/3}\right]\left\{1 + \frac{3}{4}(B_0' - 4)\left[\left(\frac{V_0}{V}\right)^{2/3} - 1\right]\right\}$$

where V_0 is the volume of the reference unit cell at ambient pressure, B_0 is the isothermal bulk modulus at ambient pressure, and B_0' is the pressure derivative of the bulk modulus extrapolated to p = 0. The fitting procedure performed by using EosFit7-GUI program[34] allowed us to determine the bulk modulus B_0 = 11.5(3) GPa and its derivative B_0' = 9.3(6) of $CsPb_2Br_5$. These parameters can be compared with those of $CsPbBr_3$. For this purpose, the single-crystal $V(p)$ data published recently for the orange form of $CsPbBr_3$[12] were fitted by the third-order Birch–Murnaghan equation (see Figure S5b) with B_0 = 15.0(8) GPa and B_0' = 6.0(18). Because B_0 and B_0' are correlated,[36] a comparison of these parameters for $CsPb_2Br_5$ and $CsPbBr_3$ was made by plotting B_0' versus B_0, together with their confidence ellipses, as illustrated in Figure S8. This plot shows that the confidence ellipses do not overlap even at the 99.7% confidence level, and therefore we conclude

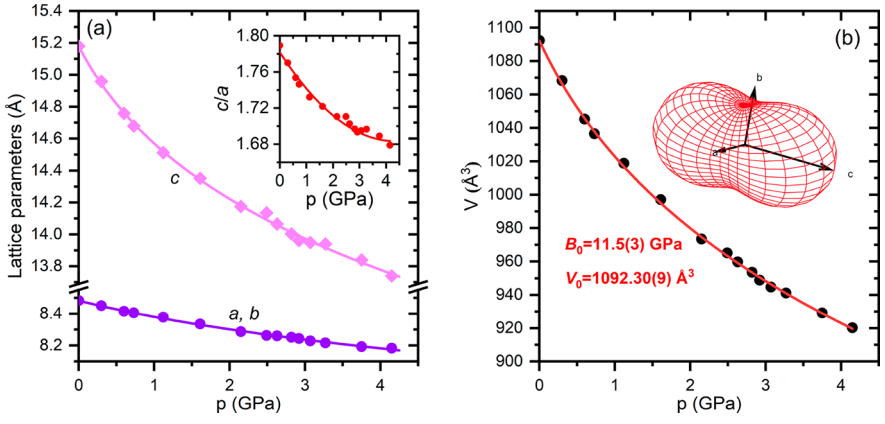

Figure 4. (a) Pressure dependence of the lattice parameters and (b) unit cell volume of $CsPb_2Br_5$. The lattice parameters and unit cell volume were fitted with the third-order Birch–Murnaghan EOS (solid lines). The inset in (b) shows the compressibility indicatrix calculated by using PASCAL software.[35]

https://doi.org/10.1021/acs.inorgchem.2c02253
Inorg. Chem. 2022, 61, 14389–14396

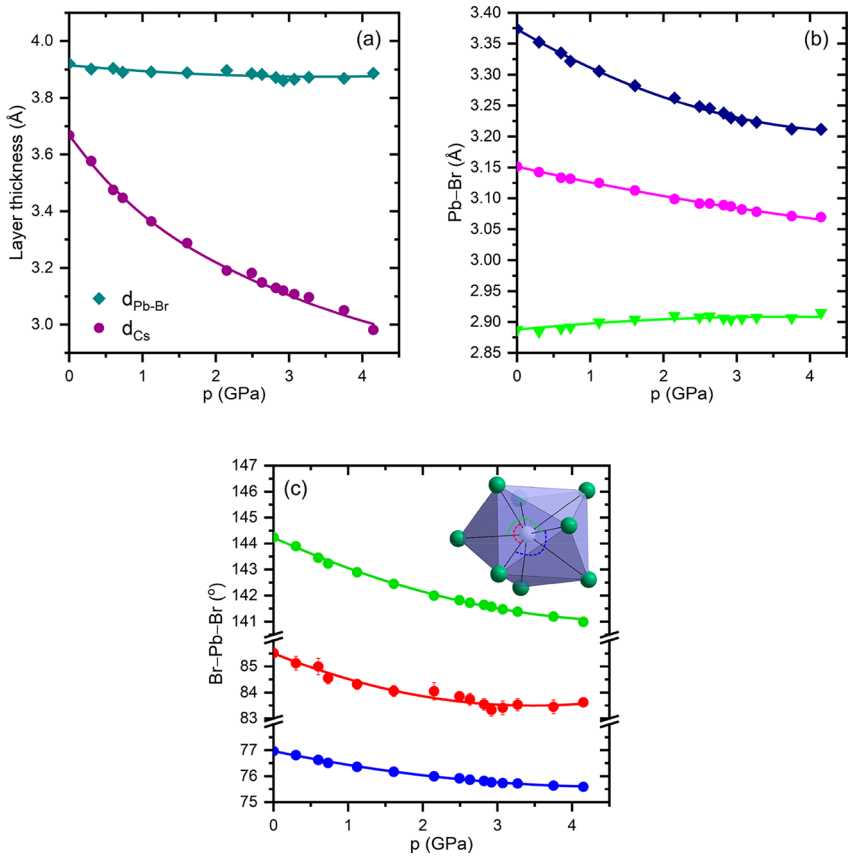

Figure 5. Pressure dependence of structural parameters in the compressed single crystal of $CsPb_2Br_5$: (a) the thickness of the Pb−Br and Cs layers, (b) the Pb−Br distances, and (c) the selected Br−Pb−Br angles; layers and Pb−Br distances are defined in Figure 1.

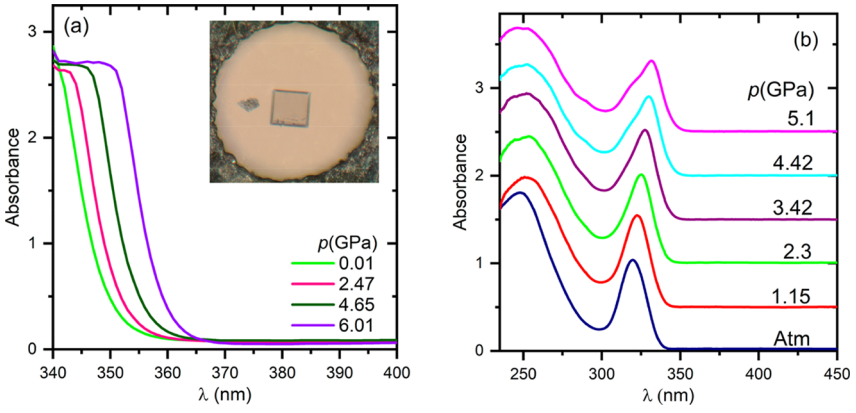

Figure 6. Selected absorption spectra of $CsPb_2Br_5$ recorded under different pressures: (a) for the 3.9 μm thick microplate and (b) for the 30 nm thick nanosheet. The inset shows the crystal in the DAC.

that the 3D perovskite $CsPbBr_3$ is less compressible than the layered $CsPb_2Br_5$. The inset in Figure 4b shows that the compressibility of $CsPb_2Br_5$ is strongly anisotropic, much higher along the c direction perpendicular to the layers than in the $a-b$ plane. It should be noted that this anisotropy varies with increasing pressure, as indicated by the nonlinear decrease in the c/a ratio (see the inset plot in Figure 4a). The linear compressibility coefficients calculated at zero pressure β_a = 14.3(8) TPa^{-1} and β_c = 61(3) TPa^{-1} were used to determine independently the bulk modulus B_0 = 11.2(6) GPa. This value is in very good accordance with that derived from the fitting of the unit-cell volume. The low value of B_0 shows that $CsPb_2Br_5$ is relatively soft as for all-inorganic material. However, this is also characteristic for 3D organic−inorganic metal halide perovskites:[37,38] for example, for $CH_3NH_3SnI_3$, B_0 = 12.6(7) GPa; for $HC(NH_2)_2SnI_3$, B_0 = 8.0(7) GPa; and for $HC(NH_2)_2PbI_3$, B_0 = 11.0(2) GPa. The other important issue is the high value of B_0', which typically is close to 4 while for $CsPb_2Br_5$ it is raised to 9.3(6). This high value is justified by the layered character of the structure as similar values were reported; for example, for graphite-like BC, B_0' = 8.0(6),[39] and for layered $GeSe_2$, B_0' = 9.1(22).[40]

In the structure of $CsPb_2Br_5$ the layers built of the face-connected bicapped trigonal prisms $PbBr_8$ are more resistant to external hydrostatic pressure than the layers composed of Cs^+ cations. This is apparent in Figure 5a, where the changes in the

https://doi.org/10.1021/acs.inorgchem.2c02253
Inorg. Chem. 2022, 61, 14389−14396

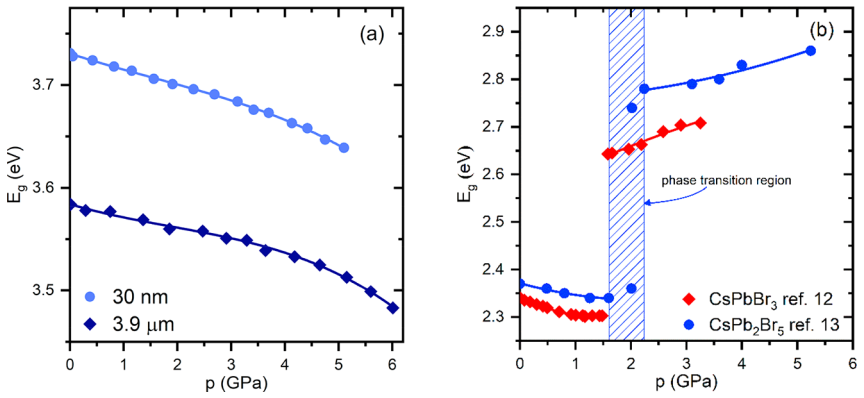

Figure 7. (a) Pressure-induced red shift of the band gap of $CsPb_2Br_5$ determined for two samples of different thickness in this work. (b) Comparison of the data reported in the literature for $CsPb_2Br_5$[13] with the results published for 3D $CsPbBr_3$.[12]

thickness of both layers are plotted as a function of pressure. In the Pb−Br layers, Pb^{2+} is coordinated by eight Br^- that form a polyhedron with three different Pb−Br distances (see Figure 1). At atmospheric pressure, these distances are strongly differentiated taking the values 3.374 Å (4×), 3.151 Å (2×), and 2.888 Å (2×). Similarly, their pressure dependences are also diversified. As shown in Figure 5b, with increasing pressure, the six longest Pb−Br bonds contract, while the two shortest bonds slightly elongate.

3.3. Absorption Edge and Energy Gap of Compressed $CsPb_2Br_5$. The absorption spectra of $CsPb_2Br_5$ were measured under pressure on a single-crystal microplate and on a nanosheet during compression cycles. The selected spectra are plotted in Figure 6. As can be seen, for the 3.9 μm thick plate only the absorption edge is accessible, while the nanosheet spectrum is structured with a well-shaped excitonic band at 320−330 nm. The absorption onset is gradually red shifted with increasing pressure. To determine the energy gap, the absorption edges were converted to Tauc plots[41] (see Figure S6) by plotting $(\alpha h\nu)^2$ versus photon energy $h\nu$, where α is the absorption coefficient of the material. The values of E_g thus obtained are plotted as a function of pressure in Figure 7a. It is evident that the band gap of $CsPb_2Br_5$ decreases monotonically with increasing pressure, without any anomalies that could be attributed to phase transitions. The $E_g(p)$ dependence is linear in the pressure range to about 4 GPa, whereas under higher pressures, beyond the hydrostatic limit of isopropanol, some nonlinearity occurs. It is not clear whether this is an intrinsic feature of the crystal or the result of nonhydrostatic conditions, which can substantially affect the properties of materials.[42,43] The character of pressure-induced changes is the same regardless of the thickness of the samples, and the only difference is that for the thicker plate the obtained value of E_g is markedly lower, but such a relation can be expected for samples of substantially different thickness, as can be deduced from the plots in Figure S7.

In the studied pressure range of 6 GPa, the overall band gap reduction is about 0.1 eV. This relatively moderate change in E_g well correlates with the subtle changes in the thickness of the compressed Pb−Br layers (Figure 5a). The calculations of the electronic band structure indicate that the band gap in $CsPb_2Br_5$ has an indirect character, but the direct gap is only slightly larger.[7] The top valence bands are composed mainly of the Br−4p, Pb−6p and Pb−6s orbitals, while the Pb−6p and Br−4p orbitals dominantly contribute to the lowest conduction bands. The orbitals of Cs^+ cations do not contribute to the electronic states responsible for the absorption edge, and therefore the largest pressure effect, visible in Figure 5a as a remarkable narrowing of the Cs^+ layers, does not have a direct translation into the optical properties of the crystal. Thus, the band gap of $CsPb_2Br_5$ is mainly determined by the structure of Pb−Br layers and its modification under pressure. As shown in Figure 5b (see also Figure 1b), crystal compression results in contraction of the six longest Pb−Br distances, while the two shortest bonds slightly elongate. The shortening of Pb−Br bonds enhances the overlap of the atomic orbitals, leading to an upward shift of the maximum valence band and, as a consequence, to a red shift of the band gap. The opposite and therefore competitive effect comes from the Br−Pb−Br angles bending.[44] The relatively small changes observed in the angles (Figure 5c) indicate that the contraction of the Pb−Br bonds has a dominant influence on the modification of the electronic states responsible for the absorption edge.

In discussing the pressure dependence of E_g, we have to refer to the data reported by Ma et al.,[13] which are plotted for comparison in Figure 7b. It is obvious that our results are in stark contrast to those obtained by Ma et al. This applies to the pressure-induced changes in the band gap as well as to its value, which is even more important. To explain these discrepancies, we plotted in Figure 7b our recently published $E_g(p)$ results measured for 3D $CsPbBr_3$.[12] The correlation between these data and the results presented by Ma et al. is evident. Therefore, we conclude that they studied, in fact, the pressure dependence of the $CsPbBr_3$ band gap instead of $CsPb_2Br_5$. Most probably, their samples were strongly contaminated with $CsPbBr_3$, and their interpretation of the results seems to be even more puzzling when considering that the same group of authors had previously published two articles on the optical properties of $CsPbBr_3$ under pressure.[45,46]

4. CONCLUSIONS

This study confirms that green photoluminescence and absorption in the visible spectrum are not intrinsic features of $CsPb_2Br_5$ but originate from $CsPbBr_3$ impurities. The microcrystallites of the orange $CsPbBr_3$ do not form inclusions embedded in the crystal plates of $CsPb_2Br_5$ but precipitate on their surfaces. Therefore, we suppose that the majority of the literature data were in fact collected for the $CsPb_2Br_5$:$CsPbBr_3$ composites instead of $CsPb_2Br_5$. We show also that the commonly used diffuse reflectance method for the absorption edge and band gap determination gives optical parameters that

https://doi.org/10.1021/acs.inorgchem.2c02253
Inorg. Chem. 2022, 61, 14389−14396

are remarkably different from those obtained from the optical absorption measurements. This discrepancy indicates that the energies of the surface and bulk electronic states of $CsPb_2Br_5$ differ significantly, which may also be characteristic for other similar materials.

Pressure was applied as a clean and effective tool to modify the distances between the atoms and bond angles and thus the related electronic structure of $CsPb_2Br_5$. Although the compressibility of this 2D perovskite-like material is larger than that of 3D $CsPbBr_3$, the pressure-induced changes in the optical parameters are smaller. The layered architecture of $CsPb_2Br_5$ is reflected in a strongly anisotropic response to hydrostatic compression. The crystal shrinks much weaker in the $a-b$ plane, i.e., parallel to the layers, than in perpendicular c direction. Furthermore, external mechanical stress affects the layers built of Cs^+ cations much more than the Pb−Br frameworks. The moderate changes within the Pb−Br layers translate into the moderate monotonic narrowing of the band gap with increasing pressure. Moreover, our study performed on the genuinely pure crystals has shown that the tetragonal structure of $CsPb_2Br_5$ is stable in a wide temperature range, at least between 90 and 625 K, and the crystal does not undergo any structural transformation in the pressure range up to 6 GPa. These results shed new light on the physical properties of $CsPb_2Br_5$ and show the interpretative pitfalls associated with the experiments performed carelessly.

■ ASSOCIATED CONTENT

Supporting Information

The Supporting Information is available free of charge at https://pubs.acs.org/doi/10.1021/acs.inorgchem.2c02253.

Selected crystallographic and refinement data, DSC and TGA results, figures illustrating experimental details, and plots illustrating a comparison to the literature data (PDF)

Accession Codes

CCDC 2176587−2176600 contain the supplementary crystallographic data for this paper. These data can be obtained free of charge via www.ccdc.cam.ac.uk/data_request/cif, or by emailing data_request@ccdc.cam.ac.uk, or by contacting The Cambridge Crystallographic Data Centre, 12 Union Road, Cambridge CB2 1EZ, UK; fax: +44 1223 336033.

■ AUTHOR INFORMATION

Corresponding Author

Marek Szafrański − *Faculty of Physics, Adam Mickiewicz University, 61-614 Poznań, Poland;* orcid.org/0000-0001-8178-5222; Email: masza@amu.edu.pl

Author

Viktoriia Drushliak − *Faculty of Physics, Adam Mickiewicz University, 61-614 Poznań, Poland;* orcid.org/0000-0003-1934-6370

Complete contact information is available at: https://pubs.acs.org/10.1021/acs.inorgchem.2c02253

Notes

The authors declare no competing financial interest.

■ ACKNOWLEDGMENTS

The authors are grateful for the financial support from the Polish National Science Centre, Grant Opus 16 No. 2018/31/B/ST3/02188. The authors also thank Prof. Marceli Koralewski for his help with the diffuse reflectance measurements and Dr. Maciej Wiesner for the determination of the crystals thickness using the AFM technique.

■ REFERENCES

(1) Tonui, P.; Oseni, S. O.; Sharma, G.; Yan, Q.; Tessema Mola, G. Perovskites Photovoltaic Solar Cells: An Overview of Current Status. *Renew. Sustain. Energy Rev.* **2018**, *91*, 1025−1044.

(2) Li, X.; Tan, Y.; Lai, H.; Li, S.; Chen, Y.; Li, S.; Xu, P.; Yang, J. All-Inorganic $CsPbBr_3$ Perovskite Solar Cells with 10.45% Efficiency by Evaporation-Assisted Deposition and Setting Intermediate Energy Levels. *ACS Appl. Mater. Interfaces* **2019**, *11*, 29746−29752.

(3) Wells, H. L. Uber Die Casium-Und Kalium-Bleihalogenide. *Z. Anorg. Allg. Chem.* **1893**, *3*, 195−210.

(4) Akkerman, Q. A.; Abdelhady, A. L.; Manna, L. Zero-Dimensional Cesium Lead Halides: History, Properties, and Challenges. *J. Phys. Chem. Lett.* **2018**, *9*, 2326−2337.

(5) Wang, K.-H.; Wu, L.; Li, L.; Yao, H.-B.; Qian, H.-S.; Yu, S.-H. Large-Scale Synthesis of Highly Luminescent Perovskite-Related $CsPb_2Br_5$ Nanoplatelets and Their Fast Anion Exchange. *Angew. Chem.* **2016**, *128*, 8468−8472.

(6) Qin, C.; Matsushima, T.; Sandanayaka, A. S. D.; Tsuchiya, Y.; Adachi, C. Centrifugal-Coated Quasi-Two-Dimensional Perovskite $CsPb_2Br_5$ Films for Efficient and Stable Light-Emitting Diodes. *J. Phys. Chem. Lett.* **2017**, *8*, 5415−5421.

(7) Tang, X.; Hu, Z.; Yuan, W.; Hu, W.; Shao, H.; Han, D.; Zheng, J.; Hao, J.; Zang, Z.; Du, J.; Leng, Y.; Fang, L.; Zhou, M. Perovskite $CsPb_2Br_5$ Microplate Laser with Enhanced Stability and Tunable Properties. *Adv. Opt. Mater.* **2017**, *5*, 1600788.

(8) Tang, X.; Han, S.; Zu, Z.; Hu, W.; Zhou, D.; Du, J.; Hu, Z.; Li, S.; Zang, Z. All-Inorganic Perovskite $CsPb_2Br_5$ Microsheets for Photodetector Application. *Front. Phys.* **2018**, *5*, 69.

(9) Wang, R.; Li, Z.; Li, S.; Wang, P.; Xiu, J.; Wei, G.; Liu, H.; Jiang, N.; Liu, Y.; Zhong, M. All-Inorganic Perovskite $CsPb_2Br_5$ Nanosheets for Photodetector Application Based on Rapid Growth in Aqueous Phase. *ACS Appl. Mater. Interfaces* **2020**, *12*, 41919−41931.

(10) Dursun, I.; de Bastiani, M.; Turedi, B.; Alamer, B.; Shkurenko, A.; Yin, J.; El-Zohry, A. M.; Gereige, I.; AlSaggaf, A.; Mohammed, O. F.; Eddaoudi, M.; Bakr, O. M. $CsPb_2Br_5$ Single Crystals: Synthesis and Characterization. *ChemSusChem* **2017**, *10*, 3746−3749.

(11) Nazarenko, O.; Kotyrba, M. R.; Wörle, M.; Cuervo-Reyes, E.; Yakunin, S.; Kovalenko, M. V. Luminescent and Photoconductive Layered Lead Halide Perovskite Compounds Comprising Mixtures of Cesium and Guanidinium Cations. *Inorg. Chem.* **2017**, *56*, 11552−11564.

(12) Szafrański, M.; Katrusiak, A.; Ståhl, K. Time-Dependent Transformation Routes of Perovskites $CsPbBr_3$ and $CsPbCl_3$ under High Pressure. *J. Mater. Chem. A* **2021**, *9*, 10769−10779.

(13) Ma, Z.; Li, F.; Qi, G.; Wang, L.; Liu, C.; Wang, K.; Xiao, G.; Zou, B. Structural Stability and Optical Properties of Two-Dimensional Perovskite-like $CsPb_2Br_5$ Microplates in Response to Pressure. *Nanoscale* **2019**, *11*, 820−825.

(14) Li, G.; Wang, H.; Zhu, Z.; Chang, Y.; Zhang, T.; Song, Z.; Jiang, Y. Shape and Phase Evolution from $CsPbBr_3$ Perovskite Nanocubes to Tetragonal $CsPb_2Br_5$ Nanosheets with an Indirect Bandgap. *Chem. Commun.* **2016**, *52*, 11296−11299.

(15) Zhang, Z.; Zhu, Y.; Wang, W.; Zheng, W.; Lin, R.; Huang, F. Growth, Characterization and Optoelectronic Applications of Pure-Phase Large-Area $CsPb_2Br_5$ Flake Single Crystals. *J. Mater. Chem. C* **2018**, *6*, 446−451.

(16) Li, J.; Zhang, H.; Wang, S.; Long, D.; Li, M.; Guo, Y.; Zhong, Z.; Wu, K.; Wang, D.; Zhang, T. Synthesis of All-Inorganic $CsPb_2Br_5$ Perovskite and Determination of Its Luminescence Mechanism. *RSC Adv.* **2017**, *7*, 54002−54007.

(17) Zhang, T.; Chen, Z.; Shi, Y.; Xu, Q. H. The Photoluminescence Mechanism of $CsPb_2Br_5$ Microplates Revealed by Spatially Resolved Single Particle Spectroscopy. *Nanoscale* **2019**, *11*, 3216−3221.

(18) Acharyya, P.; Pal, P.; Samanta, P. K.; Sarkar, A.; Pati, S. K.; Biswas, K. Single Pot Synthesis of Indirect Band Gap 2D $CsPb_2Br_5$ Nanosheets from Direct Band Gap 3D $CsPbBr_3$ Nanocrystals and the Origin of Their Luminescence Properties. *Nanoscale* **2019**, *11*, 4025−4034.
(19) Zhou, Y. Q.; Xu, J.; Liu, J. B.; Liu, B. X. Green Emission Induced by Intrinsic Defects in All-Inorganic Perovskite $CsPb_2Br_5$. *J. Phys. Chem. Lett.* **2019**, *10*, 6118−6123.
(20) Merrill, L.; Bassett, W. A. Miniature Diamond Anvil Pressure Cell for Single Crystal X-ray Diffraction Studies. *Rev. Sci. Instrum.* **1974**, *45*, 290−294.
(21) Piermarini, G. J.; Block, S.; Barnett, J. D. Hydrostatic Limits in Liquids and Solids to 100 kbar. *J. Appl. Phys.* **1973**, *44*, 5377−5382.
(22) Piermarini, G. J.; Block, S.; Barnett, J. D.; Forman, R. A. Calibration of the Pressure Dependence of the R_1 Ruby Fluorescence Line to 195 kbar. *J. Appl. Phys.* **1975**, *46*, 2774−2780.
(23) Agilent Technologies. CrysAlisPro: Data Collection and Processing Software for X-Ray Diffractometers, Santa Clara, CA, 2010.
(24) Sheldrick, G. M. A Short History of SHELX. *Acta Crystallogr. A* **2008**, *64*, 112−122.
(25) Zhang, X.; Xu, B.; Zhang, J.; Gao, Y.; Zheng, Y.; Wang, K.; Sun, X. W. All-Inorganic Perovskite Nanocrystals for High-Efficiency Light Emitting Diodes: Dual-Phase $CsPbBr_3$-$CsPb_2Br_5$ Composites. *Adv. Funct. Mater.* **2016**, *26*, 4595−4600.
(26) Turedi, B.; Lee, K. J.; Dursun, I.; Alamer, B.; Wu, Z.; Alarousu, E.; Mohammed, O. F.; Cho, N.; Bakr, O. M. Water-Induced Dimensionality Reduction in Metal-Halide Perovskites. *J. Phys. Chem. C* **2018**, *122*, 14128−14134.
(27) Yin, J.; Zhang, G.; Tao, X. A Fractional Crystallization Technique towards Pure Mega-Size $CsPb_2Br_5$ Single Crystal Films. *CrystEngComm* **2019**, *21*, 1352−1357.
(28) Murugadoss, G.; Thangamuthu, R.; Senthil Kumar, S. M.; Anandhan, N.; Rajesh Kumar, M.; Rathishkumar, A. Synthesis of Ligand-Free, Large Scale with High Quality All-Inorganic $CsPbI_3$ and $CsPb_2Br_5$ Nanocrystals and Fabrication of All-Inorganic Perovskite Solar Cells. *J. Alloys Compd.* **2019**, *787*, 17−26.
(29) Cola, M.; Massarotti, V.; Riccardi, R.; Sinistri, C. Binary Systems Formed by Lead Bromide with (Li, Na, K, Rb, Cs and Tl)Br: A DTA and Diffractometric Study. *Z. Naturforsch.* **1971**, *26*, 1328−1332.
(30) Rodová, M.; Brožek, J.; Knížek, K.; Nitsch, K. Phase Transitions in Ternary Caesium Lead Bromide. *J. Therm. Anal. Calorim.* **2003**, *71*, 667−673.
(31) Kubelka, P.; Munk, F. Ein Beitrag Zur Optik Der Farbanstriche. *Z. Technol. Physik* **1931**, *12*, 593−601.
(32) Chen, X.; Lu, H.; Yang, Y.; Beard, M. C. Excitonic Effects in Methylammonium Lead Halide Perovskites. *J. Phys. Chem. Lett.* **2018**, *9*, 2595−2603.
(33) Birch, F. Finite Elastic Strain of Cubic Crystals. *Phys. Rev.* **1947**, *71*, 809−824.
(34) Gonzalez-Platas, J.; Alvaro, M.; Nestola, F.; Angel, R. EosFit7-GUI: A New Graphical User Interface for Equation of State Calculations, Analyses and Teaching. *J. Appl. Crystallogr.* **2016**, *49*, 1377−1382.
(35) Cliffe, M. J.; Goodwin, A. L. PASCal: A Principal Axis Strain Calculator for Thermal Expansion and Compressibility Determination. *J. Appl. Crystallogr.* **2012**, *45*, 1321−1329.
(36) Anzellini, S.; Burakovsky, L.; Turnbull, R.; Bandiello, E.; Errandonea, D. P-V-T Equation of State of Iridium Up to 80 GPa and 3100 K. *Crystals* **2021**, *11*, 452.
(37) Lee, Y.; Mitzi, D. B.; Barnes, P. W.; Vogt, T. Pressure-Induced Phase Transitions and Templating Effect in Three-Dimensional Organic-Inorganic Hybrid Perovskites. *Phys. Rev. B* **2003**, *68*, No. 020103(R).
(38) Liu, G.; Kong, L.; Gong, J.; Yang, W.; Mao, H. K.; Hu, Q.; Liu, Z.; Schaller, R. D.; Zhang, D.; Xu, T. Pressure-Induced Bandgap Optimization in Lead-Based Perovskites with Prolonged Carrier Lifetime and Ambient Retainability. *Adv. Funct. Mater.* **2017**, *27*, 1604208.
(39) Solozhenko, V. L.; Kurakevych, O. O.; Solozhenko, E. G.; Chen, J.; Parise, J. B. Equation of State of Graphite-like BC. *Solid State Commun.* **2006**, *137*, 268−271.
(40) Stølen, S; Grzechnik, A; Grande, T; Mezouar, M Anisotropic Compressibility and Expansivity in Layered $GeSe_2$. *Solid State Commun.* **2000**, *115*, 249−252.
(41) Tauc, J.; Grigorovici, R.; Vancu, A. Optical Properties and Electronic Structure of Amorphous Germanium. *Phys. Status Solidi B* **1966**, *15*, 627−637.
(42) Zhang, R.; Cai, W.; Bi, T.; Zarifi, N.; Terpstra, T.; Zhang, C.; Verdeny, Z. V.; Zurek, E.; Deemyad, S. Effects of Nonhydrostatic Stress on Structural and Optoelectronic Properties of Methylammonium Lead Bromide Perovskite. *J. Phys. Chem. Lett.* **2017**, *8*, 3457−3465.
(43) Errandonea, D.; Meng, Y.; Somayazulu, M.; Häusermann, D. Pressure-Induced $\alpha \rightarrow \omega$ Transition in Titanium Metal: A Systematic Study of the Effects of Uniaxial Stress. *Physica B* **2005**, *355*, 116−125.
(44) Kong, L.; Liu, G.; Gong, J.; Hu, Q.; Schaller, R. D.; Dera, P.; Zhang, D.; Liu, Z.; Yang, W.; Zhu, K.; Tang, Y.; Wang, C.; Wei, S.-H.; Xu, T.; Mao, H.-k. Simultaneous Band-Gap Narrowing and Carrier-Lifetime Prolongation of Organic-Inorganic Trihalide Perovskites. *Proc. Natl. Acad. Sci. U. S. A.* **2016**, *113*, 8910−8915.
(45) Zhang, L.; Zeng, Q.; Wang, K. Pressure-Induced Structural and Optical Properties of Inorganic Halide Perovskite $CsPbBr_3$. *J. Phys. Chem. Lett.* **2017**, *8*, 3752−3758.
(46) Xiao, G.; Cao, Y.; Qi, G.; Wang, L.; Liu, C.; Ma, Z.; Yang, X.; Sui, Y.; Zheng, W.; Zou, B. Pressure Effects on Structure and Optical Properties in Cesium Lead Bromide Perovskite Nanocrystals. *J. Am. Chem. Soc.* **2017**, *139*, 10087−10094.

https://doi.org/10.1021/acs.inorgchem.2c02253
Inorg. Chem. 2022, 61, 14389−14396